# Magnetic tunnel junctions using LaSrMnO ferromagnetic electrodes and $PbZrTiO_3$ piezoelectric barrier

A.K. Pradhan,[a] Rajeh Mundle, Rajini B. Konda, Ozgul Yasar, Frances Williams, and Messaoud Bahoura
*Center for Materials Research, Norfolk State University, Norfolk, Virginia 23504*

(Received 22 April 2009; accepted 7 July 2009)

We report on the fabrication and tunneling characteristics of pulsed-laser deposited LaSrMnO (LSMO)/PbZrTiO(PZT)/LSMO/$SrTiO_3$ magnetic tunnel junctions. The trilayer films show magnetic onset at about 360 K with ferromagnetic hysteresis and uniaxial magnetic behavior at room temperature. The microscopic studies show that the effective barrier thickness is reduced due to the presence of defects in the barrier region. Tunneling magnetoresistance measurements were performed on several samples. Our results suggest that the asymmetric deformation of the barrier potential profile induced by the ferroelectric polarization of PZT influences the tunneling characteristics and can be used for electrically controlled readout in quantum computing schemes.

## I. INTRODUCTION

Magnetic tunnel junctions (MTJs) consisting of two ferromagnetic electrodes separated by a thin insulating barrier show large TMR making them potential candidates for memory applications. While various materials are exploited for obtaining an effective barrier for the spin-polarized tunneling, the multiferroic materials are being considered to exploit multifunctional properties in a single barrier.[1–4] A simple way to exploit this multifunctional character is to design magnetic tunnel junctions integrating a nanometric ferroelectric or piezoelectric film as the tunnel barrier. These tunnel junctions are interesting because they may exhibit effect of ferroelectric polarization on tunneling conductance[5–7] and on TMR.[8,9] The main problem is to integrate the ferroelectric–piezoelectric materials, which should have the stability of ferroelectric or piezoelectric behavior at a small thickness of a tunnel barrier. The initial results show that perovskites, such as $SrTiO_3$ (STO), show MTJ behavior when used as a tunnel barrier.[8] The purpose of the present research is to create a dynamic MTJ, in which the barrier region can further be tuned by an electric field. This allows one to study the influence of piezoelectricity of interlayer, such as $Pb(Zr_xTi_{1-x})O_3$ (PZT), on the tunneling properties that make our studies interesting compared to previously studied interlayers. This opens a next generation of multifunctional spintronic devices whose properties can be manipulated by several stimuli, as described elsewhere.[9]

Doped perovskite manganites that show ferromagnetism above room temperate[10] have received a great deal of interest because of their potential use for various device applications such as infrared detectors, magnetic field sensors,[11,12] and high density memory applications. In recent years, manganite films, such as $(La_{1-x}Sr_x)MnO_3$ (LSMO), have stimulated intense studies due to their colossal magnetoresistance (MR) effect[13,14] and spin-dependent tunneling, which makes them attractive candidates for high-performance magnetic devices. Among most of the electrofunctional perovskite oxides, the characteristics of manganite compounds are sensitive to lattice distortion imposed by chemical substitution or hydrostatic pressure. In the case of epitaxial heterostructures, a biaxial strain is induced at the interface if the lattice constant is different and the arrangement of atoms is coherent to that of the substrate. On the other hand, the strain relaxation of lattice mismatch between the film and the substrate at the interfaces occurs as the film thickness increases beyond a certain critical thickness of the film, which was recently shown in the case of LSMO.[15] The physics and the application of the doped manganites in MTJ devices based on thin-film multilayers rely on the strong dependence of their properties on strain[16–19] and their unknown interface properties.

In this work, we report on the microscopic and tunneling characteristics of a magnetic tunnel junction with manganite-based ferromagnetic electrodes, such as $La_{0.6}Sr_{0.4}MnO_3$ (LSMO) grown on STO substrates with a piezoelectric barrier, such as PZT with Zr:Ti = 65:35. We have demonstrated the MTJ behavior in LSMO/PZT/LSMO/STO multilayers.

## II. EXPERIMENTAL

All layers, LSMO/PZT/LSMO, were in situ deposited on STO substrates using the ultrahigh vacuum (UHV) pulsed laser deposition technique. Multitarget carousel is

[a]Address all correspondence to this author.
e-mail: apradhan@nsu.edu
DOI: 10.1557/JMR.2009.0378

  

used to hold the targets and position the desired target for deposition inside a vacuum chamber with a base pressure of $<2 \times 10^{-8}$ Torr. KrF excimer, ($\lambda$ = 248 nm) with a pulse energy density of 1 to 2 J/cm$^2$ was used to grow the films. The thickness of the film was precisely controlled by the number of pulses, which was predetermined from prior Rutherford backscattering and cross-sectional transmission electron micrographs. LSMO film of 55 nm of thickness is grown in 200 mT of $O_2$ at a temperature of 840 °C, followed by a thin 6 nm of PZT layer at 650 °C. The multilayer is then topped off with an additional 55-nm-thick LSMO layer deposited at 750 °C. Several samples were synthesized. However, results from two representative samples are presented here. The active device was formed by the shadow masking technique.

The current versus voltage (*I–V*) measurements were performed using an automated electrical measurement system. The polarization versus applied electric field (*P–E*) characteristic was measured at room temperature with an automated Radiant Technologies Precision LC ferroelectric test system (Albuquerque, NM).

To measure the magnetic field dependence of the MTJ, an external sample holder was inserted into the superconducting quantum interference device (SQUID) magnetometer to access the temperature variation and magnetic fields. Gold contacts were deposited, one contact on the bottom LSMO side and the other on the LSMO/PZT side. The typical sample dimension is 2 mm × 2 mm, which contains the junction area of about 0.01 mm$^2$. Further downscaling the junction area is under study. The magnetization was measured using Quantum Design MPMS-XL SQUID magnetometer (San Diego, CA) with an applied field along the surface of the film.

## III. RESULTS AND DISCUSSION

Figure 1 shows the transmission electron microscopic (TEM) images of the LSMO/PZT/LSMO/STO films. The interface is clear and sharp between the bottom LSMO and PZT, as shown in Fig. 1(a). However, the interface between PZT and the top layer LSMO is not sharp and the lattice distortions are seen within a region of about 1 nm around the interface, as shown in the inset of Fig. 1(a). A few angstroms away from the STO/LSMO interface, there are also some local misalignments of the PZT lattice. Defects in the interlayer region may be attributed to the stacking faults and even grain boundaries in the PZT layer. However, it is interesting to note that the PZT film grown on LSMO/STO films (without LSMO top layer) shows large textured grains with surface roughness of about 2 nm, confirming interface irregularities between PZT and the top layer LSMO. On the other hand, the top LSMO layer is grown at 750 °C, which affects the underneath PZT layer grown at lower temperature. It is noted that the LSMO layer grown at lower temperature shows suppressed ferromagnetic properties, which affect the tunneling.

To study the structural quality of the films, x-ray diffraction (XRD) measurements were performed. XRD studies revealed that the LSMO/PZT/LSMO/STO films contain *c*-axis oriented LSMO as well as PZT films, as presented in Fig. 1(b). Only the (00*l*) reflections of the substrate and the layers are visible, indicating good structural quality of all layers.

Figure 2 shows the temperature-dependent field-cooled (FC) and zero field-cooled (ZFC) magnetization of LSMO/PZT/LSMO/STO films. The onset of the magnetic transition was found at about $T$ = 360 K. The trilayered film demonstrates magnetic hysteresis at 250

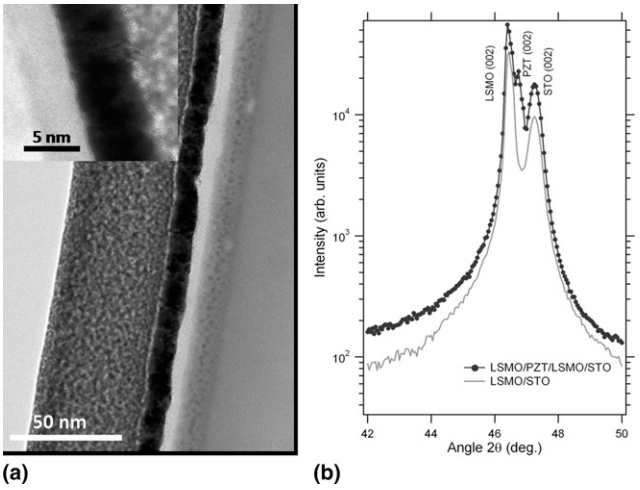


FIG. 1. (a) TEM images of the LSMO/PZT/LSMO/STO (right to left), showing interface region containing all three layers. The inset in (a) shows the HRTEM image of the PZT layer. (b) The XRD pattern of LSMO/PZT/LSMO/STO and LSMO/STO films.

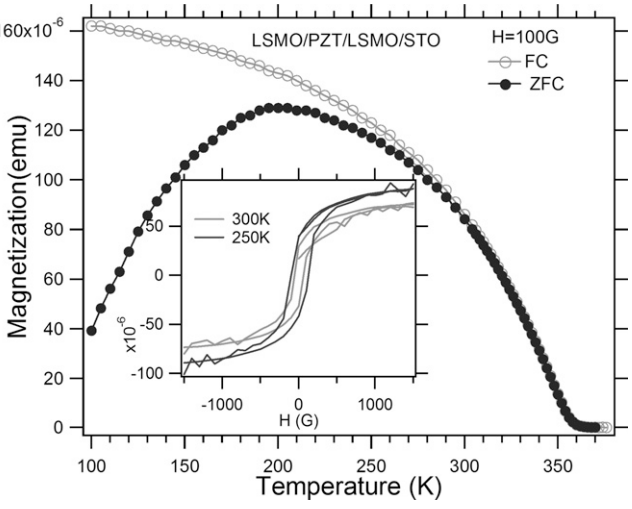


FIG. 2. Temperature dependence of ZFC and FC magnetization of the MTJ film. The inset shows the magnetization hysteresis loop of the film at two temperatures.

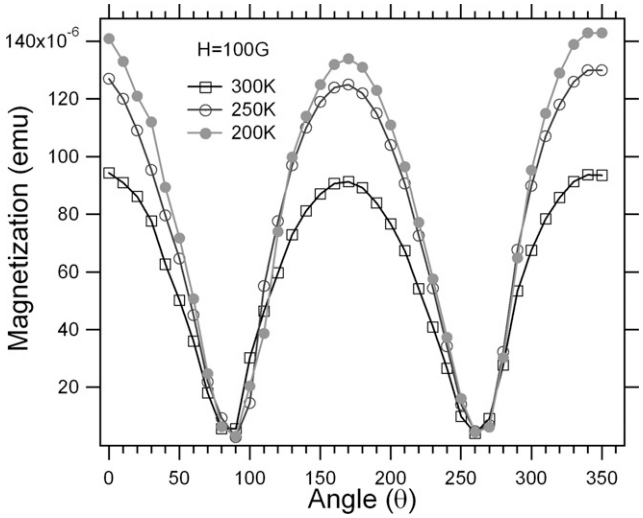


FIG. 3. Angle dependence of magnetization of LSMO/PZT/LSMO/STO films at three temperatures and at $H$ = 100 G.

and 300 K, as shown in the inset of Fig. 2. The magnetic studies clearly show that both electrodes are ferromagnetic. To know the anisotropy behavior of the multilayer film, the angle dependence of the magnetization is shown in Fig. 3 for three temperatures under a magnetic field of 100 G. It is clear from the curves that the trilayered film shows magnetic anisotropy with maximum magnetization when the surface of the film is aligned in the direction of the applied magnetic field (in-plane magnetization). It is also noted that the anisotropy behavior is weakly dependent on the temperature. Our current data suggest that the ferromagnetic layers show good magnetocrystalline behavior.

Several LSMO/PZT/LSMO/STO films were examined by electrical measurements to identify the correct tunneling behavior. The tunneling characteristics, current–voltage ($I$–$V$), of one of the junctions are shown in Fig. 4(a) at several temperatures from $T$ = 15 to 300 K. Above an absolute bias level, of which thermal smearing is minimal,[20] the trilayer junction should exhibit a vanishing $T$ dependence, which can prove whether the MTJ conduction is single electron tunneling or by conduction through a short between the two electrodes. Although $I$–$V$ characteristics show tunnel-like behavior, especially at the low-temperature region, the differential resistance (d$V$/d$I$) of MTJ does not show proposed vanishing $T$ dependence,[21,22] as shown in Fig. 4(b). The magnetic field dependence of the resistance was measured at several temperatures to investigate the tunneling magnetoresistance (TMR) of this sample. It is noted that the TMR measurements were performed with a bias voltage of 0.3 V. Figure 5 shows the TMR results of this sample at three temperatures. It is worth noting that no shift of the TMR curves was observed in both forward and reverse bias cases, although negative TMR was observed. The reason for such weak performance may be

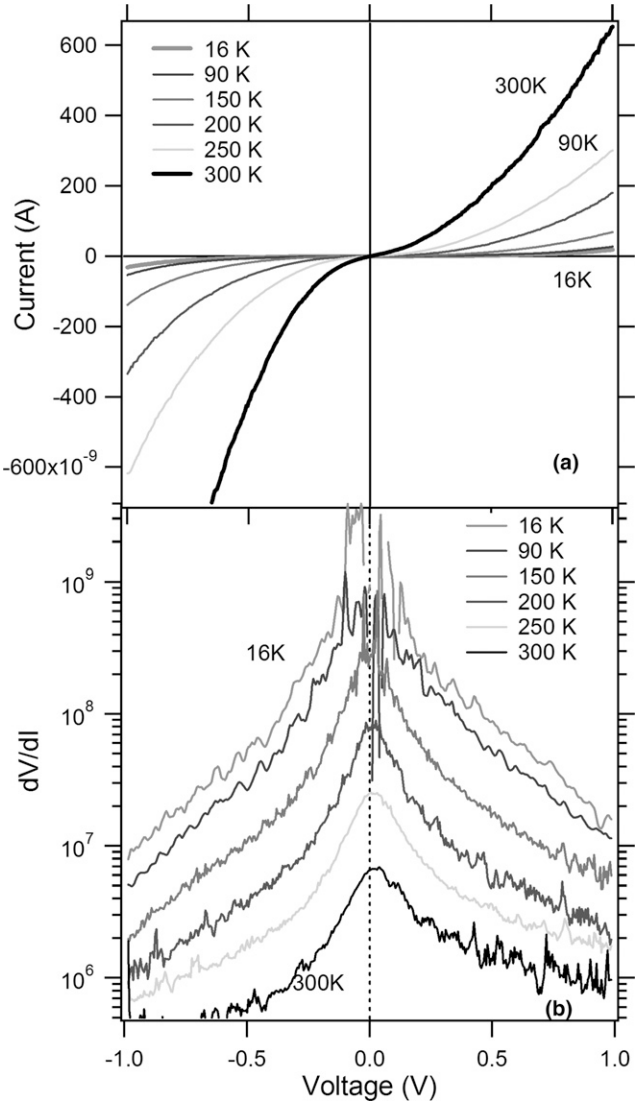


FIG. 4. (a) Current-voltage characteristics and (b) d$V$/d$I$ as a function of applied voltage of the MTJ sample 1 at various temperatures.

attributed to the low resistance (shunting) of the sample, which is probably due to high leakage through the barrier layer. The occasional presence of grain boundaries in thin barrier layer can cause such leakage.

Figures 6(a) and 6(b) show the $I$–$V$ characteristics and d$V$/d$I$ of a second MTJ sample over a wide temperature region of 5 to 320 K. The $I$–$V$ characteristics show very good tunneling-like behavior. We used the Simmon's equation[23] to fit our experimental curve to prove the tunneling behavior in our sample. Three regions, such as low, medium, and high voltage regions were considered as given below. The better fitting was observed for the barrier thickness of ~2 nm (reverse) and 1.5 nm for forward bias mode, while barrier height increases from 1.215 to 2.27 eV, respectively. This is shown in Fig. 7 for $T$ = 5 K. The modulation of the barrier height due to piezoelectric behavior of our present sample is not

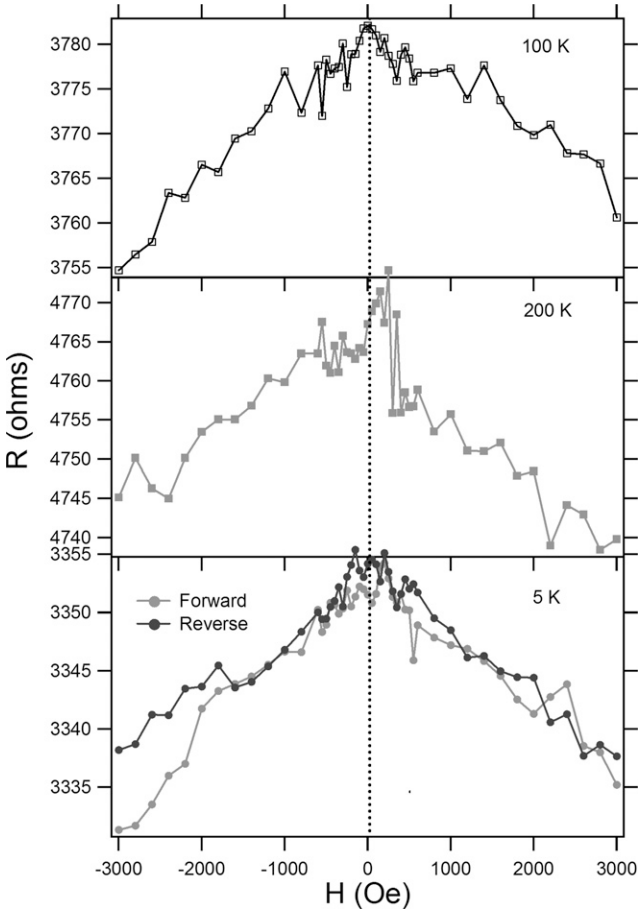


FIG. 5. TMR curves of LSMO/PZT/LSMO/STO MTJ at various temperatures.

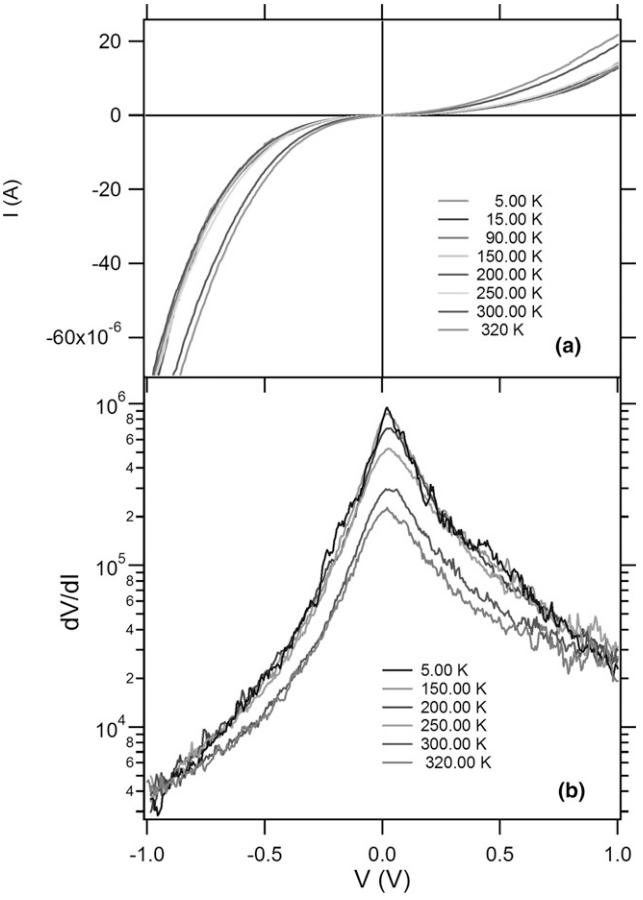


FIG. 6. (a) *I–V* characteristics and (b) d*V*/d*I* as a function of applied voltage of the MTJ sample 2 at various temperatures.

incorporated into the present fitting, and will be considered in our future study.

Low-voltage range: V ≈ 0

$$J = \frac{3(2m\varphi_0)^{1/2}}{2s}\left(\frac{e}{h}\right)^{1/2} V \times \exp\left(\frac{4\pi s}{h}(2m\varphi_0)^{1/2}\right) \quad . \quad (1)$$

Intermediate-voltage range: V < $\varphi_0$ / *e*

$$J = \left(\frac{e}{2\pi h s^2}\right)\left\{\left(\varphi_2 - \frac{eV}{2}\right)\exp\left[-\frac{4\pi s}{h}(2m)^{1/2}\right] - \left(\varphi_0 + \frac{eV}{2}\right)\exp\left[-\frac{4\pi s}{h}(2m)^{1/2}\left(\varphi_0 + \frac{eV}{2}\right)^{1/2}\right]\right\} . \quad (2)$$

High-voltage range: V > $\varphi_0$ / *e*

$$J = \left(\frac{2e^3(F/\beta)^2}{8\pi h\varphi_0}\right)\left\{\exp\left[-\frac{4\pi\beta}{eF}m^{1/2}\varphi_0^{3/2}\right] - \left(1 + \frac{2eV}{\varphi_0}\right) \times \exp\left[\frac{4\pi\beta}{eF}m^{1/2}\varphi_0^{3/2}\left(1 + \frac{2eV}{\varphi_0}\right)^{1/2}\right]\right\} \quad , \quad (3)$$

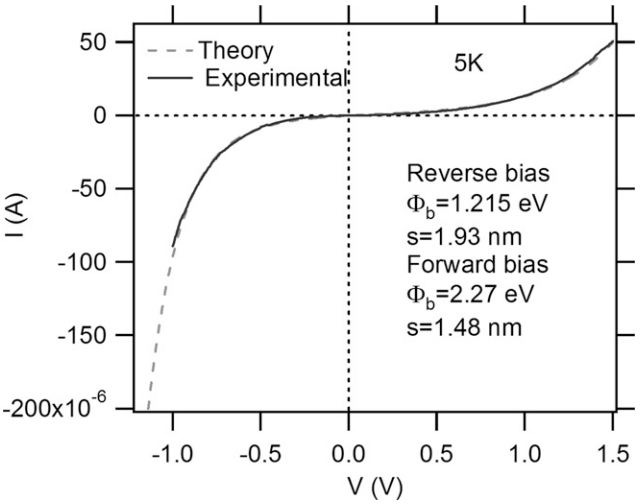


FIG. 7. *I–V* characteristics of experimental (solid) and theoretical (dotted) of the MTJ at *T*=5 K.

where *s* is the thickness of the insulating film layer, $\varphi_0$ is the height of the rectangular barrier, β is the correction factor = 23/24, and *F* = *V*/*s* is the field strength in insulator.

The fitting was found to be moderately effective for medium-voltage range, but substantial error was found near V ≈ 0. However, the present *I–V* curves exhibit the behavior of tunneling characteristics. The d*V*/d*I* curves were plotted from each *I–V* curves taken at various temperatures. The d*V*/d*I* versus *V* plot shown in Fig. 6(b), for the second MTJ sample, exhibits a vanishing *T* dependence above the absolute bias level of about 0.1 *V*, illustrating that the present sample behaves like a true MTJ. However, at the high-temperature region, the d*V*/d*I* curves did not merge well. This may be due to the effects of thermal smearing.[20]

To determine the junction characteristics, four criteria have been proposed[20–22] based on the temperature dependence and the bias voltage of the MTJ. These are (i) metal-like *R* (*T*) at all bias levels, (ii) decreasing fitted barrier height and increasing fitted barrier thickness for decreasing *T*, (iii) increased junction noise at finite bias, and (iv) increased junction instability at finite bias. These criteria were developed to fix the unreliability of Rowell criteria[21] for distinguishing tunneling from shorted samples. Rowell criteria looked at three major points, such as (i) exponential thickness dependence of the resistivity or current, (ii) parabolic shape of the differential conductance versus bias voltage, and (iii) the temperature dependence of the conductivity or resistance.[21,22] The temperature dependence of the resistance product makes for a good indicator of barrier performance, so the affects of the pinholes on the MTJ can be seen.[22] A spin-dependent tunnel barrier will make the resistance of MTJ versus temperature plot show insulator behavior, and metallic behavior when there is a short in the barrier from pinholes.[10–13] In view of the above arguments, d*V*/d*I* versus *V* plot illustrates that the present sample behaves like a true MTJ. However, TMR characteristics show strong temperature dependence, as shown in Fig. 8. The TMR remains close to 16% at 5 K compared to 5% at 300 K, as shown in the inset of Fig. 8. The TMR values sharply decline above 100 K.

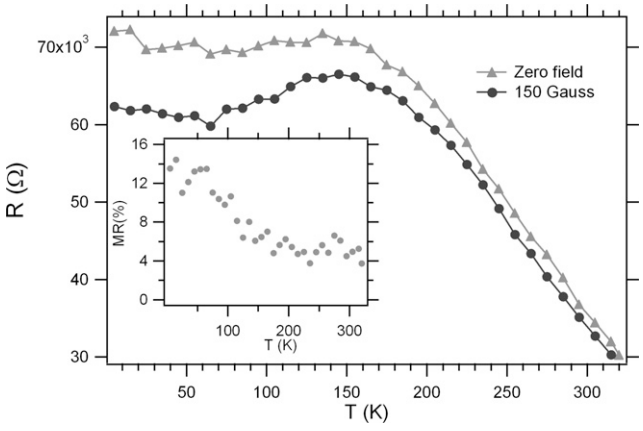


FIG. 8. TMR as a function of temperature of sample 2. The inset shows the TMR% as a function of temperature.

Figure 9 shows the TMR curves of LSMO/PZT/LSMO/STO MTJ at two temperatures. Shifting of the zero-field MR peak was prominent at 5 K, however, this feature diminishes as temperature increases. It is worth noting that the influence of the electrical polarization on tunneling has been investigated from both an experimental[8] and theoretical[9] point of view. It is expected that the modulation of the tunnel current by the polarization of the barrier is the variation of the barrier thickness owing to the converse piezoelectric effect, which produces asymmetrical current–voltage curves with a shift of the conductance minimum to a nonzero voltage.[21] On the other hand, the degradation of ferroelectricity at low thickness is a long-standing issue that has attracted much attention lately. The influence of the ferroelectric polarization is related to the charge screening at the electrode-barrier interfaces and the difference in its spatial extension at both sides of the barrier. This screening

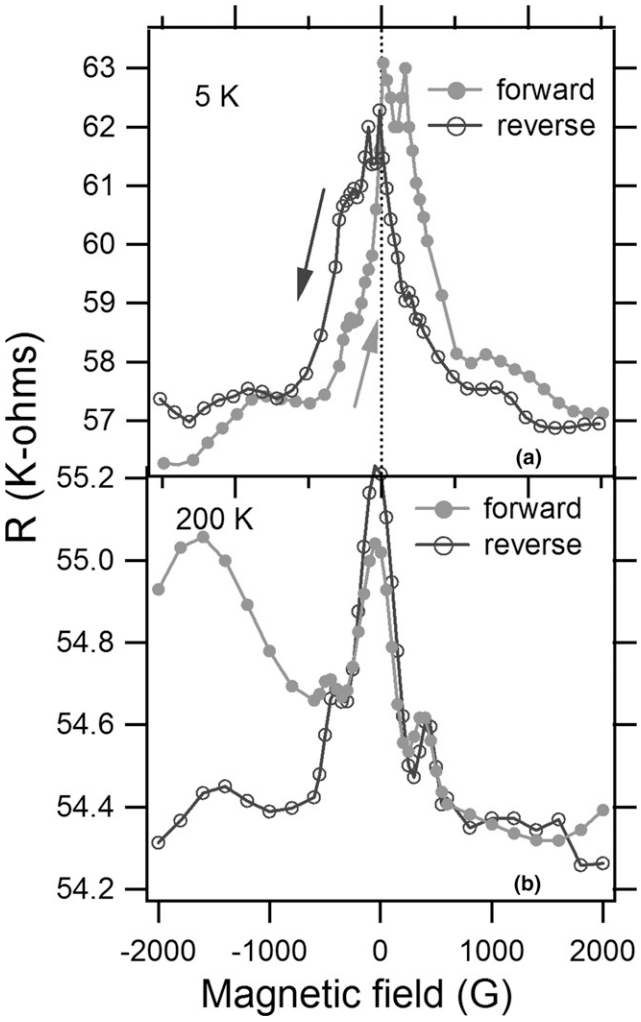


FIG. 9. TMR of sample 2 at *T* = 5 and 200 K.

controls the depolarizing field across the junction and therefore the profile of the barrier potential seen by the tunneling electrons. In addition, the formation of local current domains and electronic modifications at dislocations[16,17] are usually large and produces sharp switching, even in much thicker oxide layers (>30 nm). However, despite thin effective thickness, the films retain a ferroelectric character at room temperature and show MR close to 5% at 300 K compared to that of 16% at 5 K. It is clear that the parallel state begins at the magnetic field value at which the magnetic hysteresis loop of the MTJ reaches its saturation point and is consistent with the results shown in Fig. 9. The antiparallel state shows the higher resistive state when the magnetic field goes to zero.

Although this is indicative of the asymmetric deformation of the barrier potential profile induced by the polarization of PZT that influences the tunneling characteristics. Figure 10(a) shows the room temperature polarization versus electric field curves for the barrier PZT layer of about 5 nm to investigate the switching characteristics of the piezoelectric layer. It is obvious

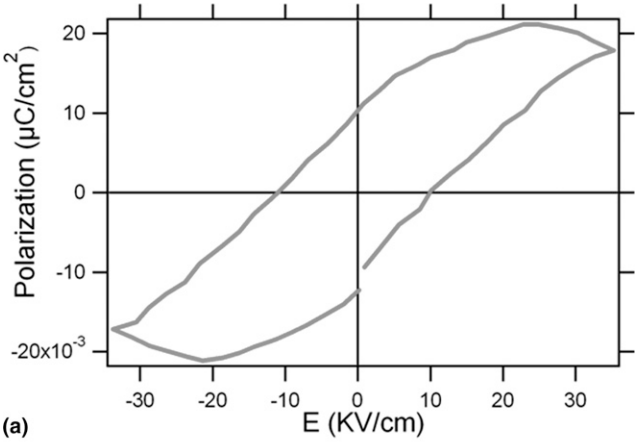


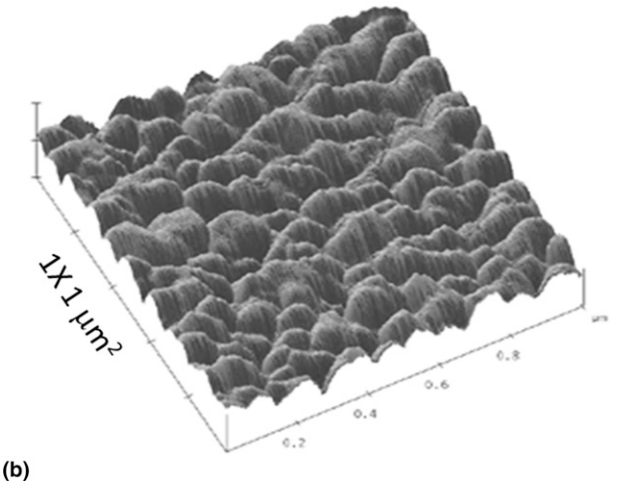


FIG. 10. (a) Polarization as a function of electric field of the barrier PZT layer at room temperature, (b) 3-dimensional atomic force microscopic image of the surface of the PZT layer.

that there is a loss/leakage above the small electric field of 15 KV/cm with saturation polarization, $P_s$ = 15 μC/cm$^2$, which is consistent with the reported value for $P_s$ in 5-nm-thick PZT film grown on $SrRuO_3$ buffered STO substrate.[4] However, the PZT layer shows large grain structures with surface roughness of 5 nm as shown in Fig. 10(b), illustrating the qualitative nature of the PZT layer. This suggests that the grain boundaries and structural defects in the PZT layer are the major reasons for the asymmetric deformation of the barrier potential, especially at the low temperature region where the polarization is expected to be strong with reduced leakage current, as shown in the previous *I–V* curves. The detailed theoretical analysis shows that the piezoelectric layer has a strong influence on the tunneling characteristics of MTJ.[24] However, further studies are needed to infer the quantitative information.

Other factors such as ferromagnetic properties of LSMO should be taken into account. The magnetic behavior of LSMO reduces rapidly above room temperature, especially when thin LSMO films are grown on a buffered layer.[16] On the other hand, it is suggested that the MR behavior at higher temperature is also influenced by the reduced magnetization of LSMO layers as observed at room temperature.

In Fig. 11, we have *I–V* curves showing the switching behavior due to the combined effect of the piezoelectric strain and depolarizing field of the LPLC magnetic tunnel junction. The biasing probe was placed on the bottom of the LSMO electrode, and the voltage was biased from −1.50 to 1.50 *V*, and then reversed. At 1.50 *V* when the voltage is reversed, we can see in the right inset that there is a drop in the current where the low resistance state becomes the high resistance state. The reverse current curve remains lower than the forward current curve down to ≈ −0.25 nA, where the current of the reverse and forward *I–V* curve cross at this first crossing point. The reverse *I–V* curve remains in a higher resistance state than the forward *I–V* curve down to −1.41 *V*. At −1.41 there is a second crossing point, where the reverse *I–V* curve changes to a lower resistance state than the forward *I–V* curve, as shown in the left inset of Fig. 11.

Ferroelectric materials have a spontaneous polarization that can be switched by an applied electric field, and this is an indicator that our insulating barrier is ferroelectric in nature.[25] The *I–V* curve of a magnetic tunnel junction with a ferroelectric barrier (FTJ) exhibits a hysteretic behavior and resistive switching. The resistive switching is a result of the sign of the piezoelectric coefficient changing, where the piezoelectric coefficient is negative when applied voltage is less than that of the coercive voltage of the ferroelectric interlayer. The piezoelectric coefficient changes sign when the coercive voltage is exceeded. The negative sign of piezoelectric coefficient below the coercive voltage is the result of the

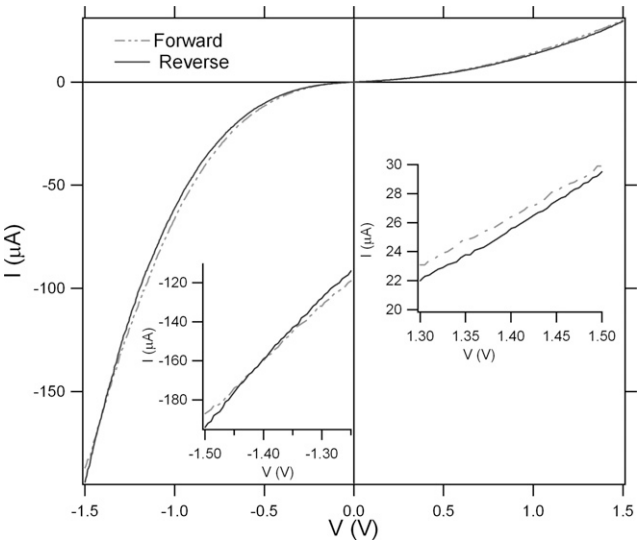


FIG. 11. *I–V* curves illustrating the switching behavior of the PZT barrier layer for forward- and reverse-bias cases at room temperature. The inset (right) shows the enlarged part of the forward bias *I–V* and the second crossing point (left), illustrating the switching phenomenon in PZT.

polarization directed against the applied field, as predicted in Ref. 26. The result of the change in sign of the piezoelectric coefficient leads to a steplike increase in the film thickness and the lattice strain. This simultaneously leads to a reduction in the barrier conductance due to the change in sign of the piezoelectric coefficient.[26] For symmetric FTJ in the negative voltage, switching the conductance drops the same as in the positive voltage switching, so the forward and reverse *I–V* curves touch at zero.

In addition to the applied electric field a field opposite in direction is formed called the depolarization field and is due to the polarization charges that form on the ferroelectric material. The mean barrier height is modified by changes in the depolarizing field, where the change can be determined. Furthermore, the magnitude and direction of the depolarizing field is dependent on the polarization of the ferroelectric material. The change in polarization of the ferroelectric material is dependent on the applied electric field. Changes in the mean barrier height modify the tunneling properties of the FTJ leading to changes in the *I–V* characteristics. In an FTJ with symmetric electrodes the electric field remains constant within the ferroelectric layer, so the change in mean barrier height is minimal. Asymmetric tunnel junctions have top and bottom electrodes with different abilities of screening the depolarizing field, so the contributions of the depolarizing field is minimal, and results in a nonzero electrostatic potential in the insulating barrier. The influence of the depolarization field modifies the mean barrier height, which results in the second crossing of the forward and reverse *I–V* curves in Fig. 11. When the applied voltage is greater than the crossing voltage of the second crossing point, the high resistance state becomes the low resistance state. In view of the above, the *I–V* curve of the present magnetic tunnel junction with a ferroelectric barrier exhibits an asymmetric hysteretic behavior and resistive switching as theoretically predicted,[26] taking into account the depolarizing field, which corresponds to the second crossing point. This confirms the present PZT-based barrier switching characteristic; however, high-quality barrier is needed to visualize the full functionalities of the MTJs. Further studies are in progress to resolve these issues.

## IV. CONCLUSION

In summary, we fabricated LaSrMnO (LSMO)/ $PbZrTiO$/LSMO/$SrTiO_3$ magnetic tunnel junctions by the pulsed laser deposition technique. The multilayered films show magnetic onset at about 360 K with ferromagnetic hysteresis, and uniaxial magnetic behavior at room temperature. The microscopic studies show that the effective barrier thickness is reduced due to the presence of defects in the barrier region. Tunneling magnetoresistance, polarization hysteresis measurements were performed on several samples. Our results suggest that the asymmetric deformation of the barrier potential profile induced by the ferroelectric polarization of PZT influences the tunneling characteristics and can be used for electrically controlled readout in quantum-computing schemes. However, further studies are necessary to fabricate a high-quality piezoelectric sandwich layer to enhance the effect.

## ACKNOWLEDGMENTS

This work is partially supported by the National Science Foundation (NSF) for Research Infrastructure in Science and Education (RISE) Grant No. HRD-0734846 and Intel Corp. The authors thank D.R. Sahu and J-L. Huang for experimental help.

## REFERENCES

1. H. Boeve, R.J.M. van de Veerdonk, B. Dutta, J. De Boeck, J. Moodera, and G. Borghs: Area scaling of planar ferromagnetic tunnel junctions: From shadow evaporation to lithographic microfabrication. *J. Appl. Phys.* **83,** 6700 (1998).
2. J.S. Moodera, L.R. Kinder, J. Nowak, P. LeClair, and R. Meservey: Geometrically enhanced magnetoresistance in ferromagnet–insulator–ferromagnet tunnel junctions. *Appl. Phys. Lett.* **69,** 708 (1996).
3. P.K. Wong, J.E. Evetts, and M.G. Blamire: High conductance magnetoresistive tunnel junctions with multiply oxidized barrier. *J. Appl. Phys.* **83,** 6697 (1998).
4. M. Gajek, M. Bibes, S. Fusil, K. Bouzehouane, J. Fontcuberta, A. Barthélémy, and A. Fert: Tunnel junctions with multiferroic barriers. *Nat. Mater.* **6,** 296 (2007).

5. M. Ye. Zhuravlev, R.F. Sabirianov, S.S. Jaswal, and E.Y. Tsymbal: Giant electroresistance in ferroelectric tunnel junctions. *Phys. Rev. Lett.* **94,** 246802 (2005).
6. J.P. Velev, C-G. Duan, K.D. Belashchenko, S.S. Jaswal, and E.Y. Tsymbal: Effect of ferroelectricity on electron transport in Pt/$BaTiO_3$/Pt tunnel junctions. *Phys. Rev. Lett.* **98,** 137201 (2007).
7. M. Ye. Zhuravlev, S.S. Jaswal, E.Y. Tsymbal, and R.F. Sabirianov: Ferroelectric switch for spin injection. *Appl. Phys. Lett.* **87,** 222114 (2005).
8. J.Z. Sun, L. Krusin-Elbaum, P.R. Duncombe, A. Gupta, and R.B. Labowitz: Temperature dependent, non-ohmic magnetoresistance in doped perovskite manganate trilayer junctions. *Appl. Phys. Lett.* **70,** 1769 (1997).
9. E.T. Wertz and Q. Li: Magnetoresistance after initial demagnetization in $La_{0.67}Sr_{0.33}MnO_3/SrTiO_3/La_{0.67}Sr_{0.33}MnO_3$ magnetic tunnel junctions. *Appl. Phys. Lett.* **90,** 142506 (2007).
10. J.P. Velev, C-G. Duan, J.D. Burton, A. Smogunov, M.K. Niranjan, E. Tosatti, S.S. Jaswal, and E.Y. Tsymbal: Magnetic tunnel junctions with ferroelectric barriers: Prediction of four resistance states from first principles. *Nano Lett.* **9,** 427 (2009).
11. A. Urushibara, Y. Moritomo, T. Arita, A. Asamitsu, G. Kido, and Y. Tokura: Insulator-metal transition and giant magnetoresistance in $La_{1-x}Sr_xMnO_3$. *Phys. Rev. B* **51,** 14103 (1995).
12. J. Heremans: Solid state magnetic field sensors and applications. *J. Phys. D: Appl. Phys.* **26,** 1149 (1993).
13. S. Jin, M. McCormack, T.H. Tiefel, and R. Ramesh: Colossal magnetoresistance in La–Ca–Mn–O ferromagnetic thin films. *J. Appl. Phys.* **76,** 6929 (1994).
14. J. Fontcuberta, B. Martinez, A. Seffer, S. Pinol, J.L. Garcia-Munoz, and X. Obaradors: Colossal magnetoresistance of ferromagnetic manganites: Structural tuning and mechanisms. *Phys. Rev. Lett.* **76,** 1122 (1996).
15. J-Q. Wang, R.C. Barker, G-J. Cui, T. Tamagawa, and B.L. Halperm: Doped rare-earth perovskite Mn films with colossal magnetoresistance. *Appl. Phys. Lett.* **71,** 3418 (1997).
16. A.K. Pradhan, D. Hunter, T. Williams, B. Lasley-Hunter, R. Bah, H. Mustafa, R. Rakhimov, J. Zhang, D.J. Sellmyer, E.E. Carpenter, D.R. Sahu, and J-L. Huang: Magnetic properties of $La_{0.6}Sr_{0.4}MnO_3$ thin films on $SrTiO_3$ and buffered Si substrates with varying thickness. *J. Appl. Phys.* **103,** 023914 (2008).
17. A. Wiedenhorst, C. Höfener, Y. Lu, J. Klein, M.S.R. Rao, H. Freitag, W. Mader, L. Alff, and R. Gross: High-resolution transmission-electron-microscopy study on strained epitaxial manganite thin films and heterostructures. *J. Magn. Magn. Mater.* **211,** 16 (2000).
18. M. Izumi, Y. Murakami, Y. Konishi, T. Manako, M. Kawasaki, and Y. Tokura: Structure characterization and magnetic properties of oxide superlattices $La_{0.6}Sr_{0.4}MnO_3/La_{0.6}Sr_{0.4}FeO_3$. *Phys. Rev. B* **60,** 1211 (1999).
19. A.K. Pradhan, D. Sahu, B.K. Roul, and Y. Feng: $La_{1-x}Ba_xMnO_3$ epitaxial thin films by pulsed laser deposition: A consequence of strain stabilization. *Appl. Phys. Lett.* **81,** 3597 (2002).
20. A.K. Pradhan, S. Mohanty, K. Zhang, J.B. Dadson, E.M. Jackson, D. Hunter, R.R. Rakhimov, G.B. Loutts, J. Zhang, and D.J. Sellmyer: Integration of epitaxial colossal magnetoresistive films onto Si(100) using $SrTiO_3$ as a template layer. *Appl. Phys. Lett.* **86,** 012503 (2005).
21. J.J. Akerman, I.V. Roshchin, J.M. Slaughter, R.W. Dave, and I.K. Schuller: Origin of temperature dependence in tunneling magnetoresistance. *Europhys. Lett.* **63,** 104 (2003).
22. J.J. Akerman, J.M. Slaughter, R.W. Dave, and I.K. Schuller: Tunneling criteria for magnetic-insulator-magnetic structures. *Appl. Phys. Lett.* **79,** 3104 (2001).
23. D.A. Rabson, B.J. Jönsson-Åkerman, R. Escudero, C. Leighton, S. Kim, and I.K. Schuller: Pinholes may mimic tunneling. *J. Appl. Phys.* **89,** 2786 (2001).
24. J.G. Simmons: Generalized formula for the electric tunnel effect between similar electrodes separated by a thin insulating film. *J. Appl. Phys.* **34,** 1793 (1963).
25. V. Nagarajan, J. Junquera, J.Q. He, C.L. Jia, R. Waser, K. Lee, Y.K. Kim, S. Baik, T. Zhao, R. Ramesh, Ph. Ghosez, and K.M. Rabe: Scaling of structure and electrical properties in ultrathin epitaxial ferroelectric heterostructures. *J. Appl. Phys.* **100,** 051609 (2006).
26. H. Kohlstedt, N.A. Pertsev, J. Rodríguez Contreras, and R. Waser: Theoretical current-voltage characteristics of ferroelectric tunnel junctions. *Phys. Rev. B* **72,** 125341 (2005).